Rashba effect in type-II resonant tunneling diodes enhanced by in-plane magnetic fields

J. Silvano de Sousa* and J. Smoliner

Institute of Solid State Electronics, Vienna University of Technology (TU-Wien), Floragasse 7, A-1040 Vienna, Austria

(Received 15 November 2011; published 8 February 2012)

In this paper, we adapt the transfer matrix method to calculate the current-voltage curves of type-II GaAsSb/InGaAs resonant tunneling diodes on which a huge Rashba splitting of the current resonances has been reported recently. It is shown that, in transverse magnetic fields, the $k_\parallel$ distribution of tunneling electrons is shifted to higher values. Through this process, a significant asymmetry is induced in the tunneling structure, which finally leads to a strong enhancement of the Rashba effect. Further, we find that the Rashba effect is extremely sensitive to the electric fields produced by the band discontinuities at the heterostructure interfaces and to the spin-orbit coupling constants in the respective materials. Using a one-band model for the spin-orbit coupling constant, the effects of temperature and local electric fields on the Rashba parameter are also investigated. From our findings, we conclude that spin-splitting effects and large spin-orbit interactions should be quite dominant in any narrow-gap type-II heterostructure, and not only in the GaAsSb/InGaAs material system.

DOI: 10.1103/PhysRevB.85.085303 PACS number(s): 71.70.Ej, 73.40.Gk, 73.20.−r, 75.76.+j

I. INTRODUCTION

The control of the spin degree of freedom is a key point for developing functional devices in semiconductor spintronics.[1–3] The use of gate voltages or designed structures instead of magnetic fields in order to lift spin degeneracy would be preferred.[4,5] For this specific task, spin-orbit (SO) interaction effects are the most promising way to achieve total spin manipulation in semiconductor heterostructures. In the two-dimensional (2D) case, the spin-orbit coupling due to structural inversion asymmetry known simply as the "Rashba effect"[6,7] is of advantage. The energy dispersion relation for a 2D system with Rashba spin-orbit coupling is given by $E_\pm = E_z + (\hbar k_\parallel)^2/2m^* \pm \alpha k_\parallel$, where each sign corresponds to a spin state for a given wave vector $k_\parallel$. The parameter α is the material-dependent Rashba spin-orbit coupling constant which includes all spin-orbit mechanisms in the system.

II. RASHBA EFFECT IN RESONANT TUNNELING

In our most recent work,[8] we demonstrated experimentally how a transverse magnetic field can be used to determine the Rashba parameter α in InGaAs/GaAsSb double-barrier resonant tunneling diodes (RTDs). In the perpendicular transport case, the in-plane magnetic field is used to accelerate the tunneling electrons parallel to the barrier planes via Lorentz forces. Figure 1 shows a qualitative sketch of the RTD conduction band with the current and magnetic field directions indicated. The increase of the in-plane momentum $k_\parallel$ enhances the Rashba effect ($E\uparrow - E\downarrow = 2\alpha k_\parallel$) in the quantum well (QW), which results in the splitting of the characteristic RTD's current resonance into two.

The mechanism that causes the enhancement of the Rashba effect in InGaAs/GaAsSb RTDs can be qualitatively understood in Fig. 2. The filled parabolas represent the emitter states and the two separated open parabolas represent the Rashba levels in the quantum well. When $B = 0$ [Fig. 2(a)], the electrons do not gain any in-plane momentum while tunneling from the emitter into the quantum well. This can be represented graphically by centering the emitter parabola at $k_\parallel = 0$. When the tunneling condition is reached [position 2 in Fig. 2(a)], the emitter parabola overlaps both Rashba parabolas in the quantum well simultaneously and no splitting is seen [position 2 in lower curve of Fig. 2(b)]. When $B > 0$, the tunneling electrons gain in-plane momentum and the emitter parabola is centered at $k_\parallel \neq 0$ [Fig. 2(a)]. This asymmetry in $k_\parallel$ space allows the emitter parabola to overlap each Rashba parabola separately [positions 2 and 3 in Fig. 2(a) for $B > 0$], producing, thus, the peak splitting observed in the upper curve of Fig. 2(b) ($B > 0$). The energy separation between the split resonance peaks caused by the shift in in-plane momentum given by the magnetic field yields the Rashba parameter. The experimental values for the Rashba parameter in these structures range from 0.38 to 0.75 eVÅ for well widths between 7 and 20 nm (see Ref. 8).

In order to get a more quantitative understanding of the observed results, we calculated the tunneling current using the Esaki-Tsu model.[9] All scattering effects were neglected and the electron transport was assumed to be completely ballistic. The transmission coefficient was calculated via the transfer matrix formalism, where the influences of the transverse magnetic field and of the Rashba effect on the in-plane energies are taken into account in a semiclassical picture. Nonparabolicity effects in the quantum well[10] are taken into account via a two-band Kane model[11] $m^*(E) = m_0^*(1 + 2\frac{E}{E_{\text{gap}}})$, where m_0^* is the bulk effective mass and E is the energy above the conduction band. For the Rashba parameter calculation we used the one-band model developed by de Andrada e Silva, La Rocca, and Bassani.[12] The temperature dependence of the Rashba parameter is implemented in the calculation via the temperature-dependent band gaps of the involved materials.

III. CALCULATION OF THE TUNNELING CURRENT

For the calculations we used a typical sample with 9-nm-thick barriers and a 13-nm-long quantum well. The magnetic field is set in the plane of the barriers and the current is considered to flow from left to right in the z direction (see Fig. 1). As usual, we assume ballistic transport in the active region of the RTD and e-e and e-phonon scattering

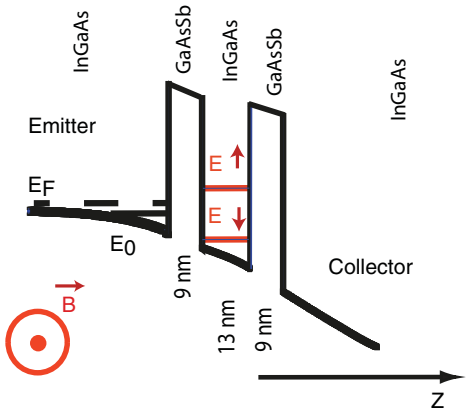

FIG. 1. (Color online) Sketch of the biased RTD's conduction band with indication of the current flow and magnetic field directions. $E\uparrow$ and $E\downarrow$ correspond to the spin states.

processes are neglected. The tunneling current density is given by $j = evn$, where e is the elementary charge, v is the tunneling velocity, and n is the transmitted electron density. The transmitted current density can be written in terms of the wave number k by using the relation $v = \frac{\hbar k}{m^*}$. In order to calculate the transmitted electron density, we assume a two-dimensional emitter electrode with one occupied subband only. The sheet density of transmitted electrons [Eq. (1)] is the integral in k space of the product of the density of states $D(k_\parallel)$ and the transmission coefficient T of the tunneling structure weighted by the Fermi distribution,

$$n^{2D} = \int_0^\infty D(k_\parallel) f(k_\parallel) T(k_z, k_\parallel; V; B_{||}) dk_\parallel. \quad (1)$$

In order to calculate the current density, an electron concentration per volume unit is needed. This can be determined assuming $n^{3D} = (n^{2D})^{2/3}$.

We obtain the value of k_F from the 2D carrier density in the emitter, which we estimate by using a parallel-plate capacitor model under external bias:

$$en^{2D} = \frac{Q}{A} = \frac{\varepsilon\varepsilon_0 V}{d}, \quad (2)$$

where A is the area of the device, V the applied bias, ε the dielectric constant, and d the distance between the RTD and the highly doped back contact region. For the bias-dependent transmission coefficient, the band profile was first calculated at zero bias by solving the Poisson equation numerically.[13] For biased structures, a linear voltage drop between the emitter and the collector contact was assumed. After this, it is straightforward to determine the Fermi energy and the corresponding Fermi vector in the emitter side:

$$E_F^{2D} = \frac{\pi\hbar^2}{em^*}\frac{\varepsilon\varepsilon_0 V}{d}, \quad k_F = \sqrt{\frac{2m^* E_F^{2D}}{\hbar^2}}. \quad (3)$$

Now, all that is needed for the calculation of the tunneling current is the determination of the transmission coefficient T including the influences of the magnetic field and the Rashba effect.

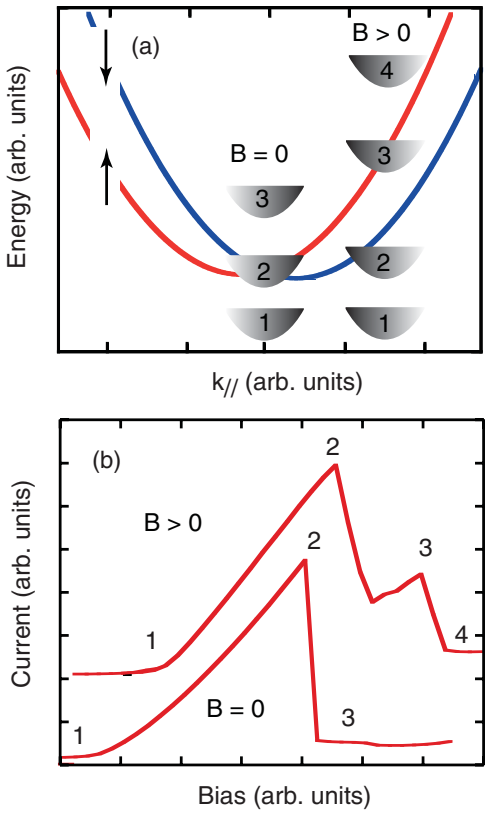

FIG. 2. (Color online) Rashba effect enhancement in double-barrier RTDs. For $B = 0$ (a), the emitter parabola is centered at $k = 0$ and overlaps both Rashba states in the quantum well simultaneously during resonance [step 2 of the lower curve in (b)]. For $B > 0$, the emitter parabola is centered at $k > 0$ and thus it can overlap each Rashba state separately. This results in two resonance peaks represented by steps 2 and 3 of the upper curve in (b). The resonances shown in (b) are actual experimental data for a RTD with a 13 nm well.

IV. SPIN-DEPENDENT TRANSMISSION COEFFICIENTS

A. The influence of transverse magnetic fields

To consider the effects of a magnetic field, the transmission coefficient $T(k_z)$ must be accordingly adapted. This calculation can be done conveniently in a semiclassical way. For instance, if the magnetic field is set in the x direction (B_x), the k_y and k_z components of the electron's momentum are coupled while k_x stays unaffected. The acting Lorentz force transfers the electron's momentum from the z to the y direction. Quantitatively, k_y increases by $\delta k_y = \frac{eB_x}{\hbar}\delta z$ where $\delta z = (z - z_0)$ denotes the distance traveled in the magnetic field. In other words, k_y can be expressed as a function of the electron's position:

$$k_y(z) = k_y^0 + \frac{eB_x}{\hbar}(z - z_0), \quad (4)$$

where k_y^0 is the initial wave vector component in the y direction. The corresponding components of the kinetic energy (E_z and E_y) change continuously while the total energy $E = E_z + E_y + E_x$ is conserved. Figure 3 shows qualitatively the effect of a transverse magnetic field (B_x) on the trajectory of an electron. If the initial value of k_y is zero or negative, the

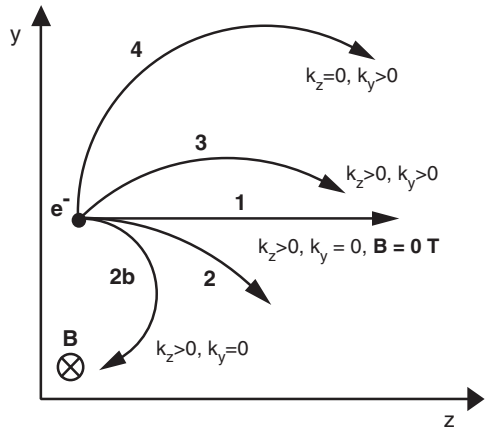

FIG. 3. Classical trajectories of electrons in a magnetic field. Curve 1 shows a trajectory without the influence of a magnetic field; the other trajectories are influenced by a magnetic field parallel to the x axis. k_z and k_y denote the initial values of the momentum components. Trajectories 2 and 2b have the same initial momentum, but in the case of 2b the magnetic field is larger.

electron always loses E_z and gains E_y (see trajectories 2 and 2b), whereas for a positive initial value of k_y, as is clear from trajectories 3 and 4, the electron first gains and then loses E_z. Trajectory 4 shows the extreme case of $k_z = 0$.

B. Spin-dependent transmission coefficient

The Rashba effect is included in the transmission coefficient calculation after the addition of the spin-orbit coupling term $H_{\mathrm{SO}} = \pm\alpha k_{\parallel}$ to the in-plane energies in the QW. Minor contributions due to the inversion asymmetry of the bulk host material[14,15] and Zeeman splitting[8] are considered negligible and not taken into account. For the calculation, the parameter α is considered to be nonzero only in the quantum well. After using the result from Eq. (4), the z-dependent in-plane energy reads

$$E(k_{\parallel}^{\pm}(z)) = \frac{\hbar^2 k_{\parallel}^2(z)}{2m^*(z)} \pm \alpha k_{\parallel}(z) \quad \text{with } k_{\parallel}(z) = \sqrt{k_x^2 + k_y^2(z)}. \tag{5}$$

Finally, the spin-dependent momentum $k_z^{\pm}$ is written in terms of the electron's position z:

$$k_z^{\pm} = \sqrt{\frac{2m^*(z)}{\hbar^2}[E - U(z) \mp \alpha(z)k_{\parallel}(z)] - k_{\parallel}^2(z)}, \tag{6}$$

where E is the total energy and $U(z)$ is the conduction band potential. Note that the addition of the Rashba term will imply two distinct values for the transmission coefficient: one for spin down $(-)$ and the other for spin up $(+)$.

With the result of Eq. (6), the spin-dependent transmission coefficient can be calculated via the transfer matrix method[16,17] (TMM), with a spin-dependent transfer matrix $M\pm$:

$$\begin{pmatrix} A_{\pm}^R \\ B_{\pm}^R \end{pmatrix} = M_{\pm} \begin{pmatrix} A_0^L \\ B_0^L \end{pmatrix}, \tag{7}$$

where $A_{\pm}^R$ and $B_{\pm}^R$ are the amplitudes of the spin-polarized wave functions on the right side of the quantum well and A_0^L and B_0^L are the amplitudes of the nonpolarized wave functions on the left side. The spin-dependent transfer matrix $M_{\pm}$ is the product of all transfer matrices associated with each point of the discretized potential structure:

$$M_{\pm} = \prod \begin{pmatrix} (a^i P)_{\pm} & (b^i Q)_{\pm} \\ (b^i Q^*)_{\pm} & (a^i P*)_{\pm} \end{pmatrix}, \tag{8}$$

where

$$a^i = \frac{1}{2}\left\{1 + \frac{m^{*(i+1)}}{m^{*(i)}}\frac{k_z^{\pm(i)}}{k_z^{\pm(i+1)}}\right\},$$

$$b^i = \frac{1}{2}\left\{1 - \frac{m^{*(i+1)}}{m^{*(i)}}\frac{k_z^{\pm(i)}}{k_z^{\pm(i+1)}}\right\},$$

$$P = \exp\left\{i\left(k_z^{\pm(i)} - k_z^{\pm(i+1)}\right) z_{i+1}\right\},$$

$$\text{and} \quad Q = \exp\left\{i\left(k_z^{\pm(i)} + k_z^{\pm(i+1)}\right) z_{i+1}\right\}.$$

The spin-dependent transmission coefficient $T_{\pm}$ is given by

$$T_{\pm} = \frac{m^{*L}}{m^{*R}}\frac{k^R}{k^L}\frac{|A_{\pm}^R|^2}{|A_0^L|^2}. \tag{9}$$

V. THE RASHBA PARAMETER AND TEMPERATURE DEPENDENCE

For the calculation of the Rashba coefficient, we follow the publications by de Andrada e Silva and co-workers,[12,18] who showed that the Rashba parameter can be written as the product of a material-dependent coefficient α_{SO} with the electric field throughout the quantum well, $\mathcal{E}_{\mathrm{ext}}$, including the fields at the interfaces that result from the band discontinuity $\mathcal{E}_I = dE_v/dz$:

$$\alpha(z) = \alpha_{\mathrm{SO}}\frac{d(E_v + V_{\mathrm{ext}})}{dz}, \tag{10}$$

$$\text{where} \quad \alpha_{\mathrm{SO}} = e\frac{\hbar^2}{2m^*}\frac{\Delta}{E_g}\frac{2E_g + \Delta}{(E_g + \Delta)(3E_g + 2\Delta)}. \tag{11}$$

Note that, for the calculation of the Rashba coefficient, the field in the valence band must be used.[19] Since detailed values for the spin-orbit gap Δ in GaAsSb do not exist in the literature, we assumed the spin-orbit splitting in GaSb (Ref. 18) ($\Delta = 0.75$ eV), which will be a reasonably good approximation since the formula is relatively insensitive to the exact value of Δ. The Rashba parameter is especially large at the heterointerfaces, where the potential E_v changes significantly over one atomic layer, resulting in extremely large electric fields. In this effective-mass picture, the electric field produced is the ratio of the band offset in the valence band to the effective width of the interface. Further, α can be positive or negative depending on the electric field direction at the interface. The interface width is assumed to be on the order of the distance between two crystal planes, which is half of the lattice constant in GaAsSb (0.586 nm).

The validity of this one-band approximation for the Rashba spin-orbit coupling parameter [Eq. (11)] has been discussed in Ref. 12, where the one-band α_{SO} yields smaller spin splitting energies than the full α_{SO} calculation. Nevertheless, it will become evident in the results of our calculations that this simplified model is sufficient to produce good agreement between the simulation and the experiment.

Even though they are not apparent, the effects of fields produced by the band discontinuities are still present in the one-band approximation for the Rashba parameter [Eq. (11)]. It can be demonstrated if one applies the proper approximations after differentiating Eq. (5) of Ref. 12, which gives

$$\frac{d\beta}{dz} = \frac{P^2}{2}\left[\left(\frac{1}{\varepsilon_\pm - V_{\rm ext}(z) - E_v(z)}\right)^2 - \left(\frac{1}{\varepsilon_\pm - V_{\rm ext}(z) - E_v(z) + \Delta}\right)^2\right]\frac{d[E_v(z) + V_{\rm ext}(z)]}{dz}, \quad (12)$$

where the $\alpha_{\rm SO}$ coefficient can be identified. The $\alpha_{\rm SO}$ term in Eq. (12) can be rewritten in terms of the effective-mass expression given by Eq. (16) in Ref. 12:

$$\alpha_{\rm SO} = \frac{\hbar^2}{2m^*}\frac{E_g(E_g+\Delta)}{3E_g+2\Delta}\left[\left(\frac{1}{\varepsilon_\pm - V_{\rm ext}(z) - E_v(z)}\right)^2 - \left(\frac{1}{\varepsilon_\pm - V_{\rm ext}(z) - E_v(z) + \Delta}\right)^2\right]. \quad (13)$$

The expansion parameter δ used in Ref. 12 yields

$$\delta(E_g + \Delta) + E_c(z) = \varepsilon_\pm - V_{\rm ext}(z). \quad (14)$$

After inserting Eq. (14) into Eq. (13) and considering $\delta(E_g + \Delta) \ll E_g$, one acquires the expression for $\alpha_{\rm SO}$ given by Eq. (11).

The temperature dependence of the Rashba parameter is included in the calculations via the band-gap energy. The energy gap can be calculated as function of the temperature via the Varshni formula[20]

$$E_{\rm gap}(T) = E_{\rm gap}(0) - \frac{\tilde{\alpha}T^2}{\beta + T}. \quad (15)$$

For InGaAs, $\tilde{\alpha} = 4.19 \times 10^{-4}$ and $\beta = 271$ (see Refs. 21 and 22) and we have $\tilde{\alpha} = 13.5 \times 10^{-4}$ and $\beta = 135$ (see Ref. 23) for GaAsSb.

As we know of no experimental data on the temperature dependence of the band offsets in this material in the literature, we assumed that the ratio between the band discontinuity and the band gap stays constant for all temperatures.

VI. RESULTS

A. Simulated currents

We now discuss the results of our simulations. Figure 4 shows the simulated $I(V)$ curves for a 13 nm RTD quantum well under magnetic fields of $B = 0$, 1, 2, 3, and 4 T at $T = 4$ K. The parameters used in the calculation are displayed in Fig. 9(b). For better clarity, only the bias range around the resonance is shown. As expected, at $B = 0$ T no peak splitting is observed. The deviation from a symmetric Gaussian-type resonance peak is due to the influence of nonparabolicity effects. With increase of the magnetic field, the Rashba effect starts to influence the in-plane energies in the quantum well and the resonance is split into two peaks. The first peak is associated with the spin-down electrons and the second with the spin-up electrons. Note that the Rashba effect causes the first peak to move backward on the bias axis for low magnetic fields. For high magnetic fields, though, both peaks are shifted to higher biases as the change in the in-plane kinetic energy term $\frac{\hbar^2 k_\parallel^2(z;B)}{2m^*}$ [see Eq. (5)] starts to play a more important role in the tunneling energies. The overall peak positions and splitting sizes are in excellent agreement with the experimental results (see Ref. 8).

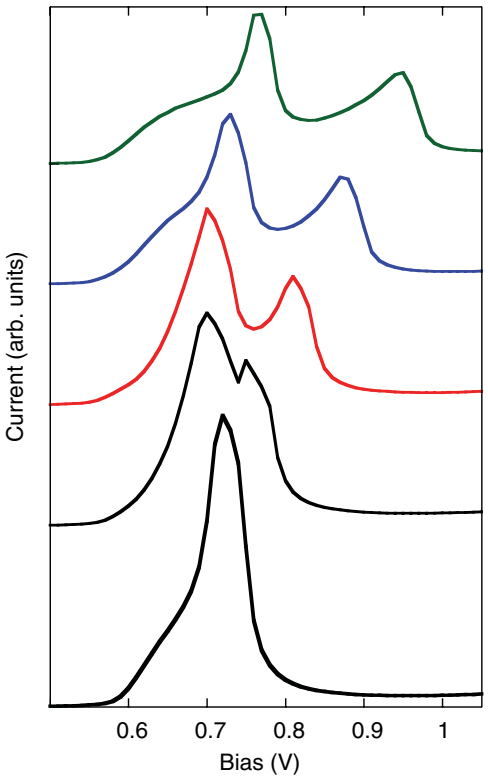

FIG. 4. (Color online) Simulated $I(V)$ curves for magnetic fields $B = 0$, 1, 2, 3, and 4 T. For a better presentation, a current offset is added to the $I(V)$ curves at $B \neq 0$ T. For the parameters used here, please check Fig. 9(b).

B. Spin polarization

In the RTD case, spin polarization is achieved in the cases where anisotropy is present in the lateral momentum of electron undergoing resonant tunneling.[24–26] In our case, this anisotropy is created by the in-plane magnetic field.

Each of our calculated $I(V)$ curves is the sum of the corresponding spin-up (T_+) and spin-down (T_-) currents, where the $\pm$ sign refers to the spin up and down along the x direction. The contribution of each spin current and their sum are shown in Fig. 5 for $B = 2$ T and $T = 4$ K. The spin polarization degree of each current peak can be defined in a similar way as in Refs. 12 and 25. Here, it is defined as the ratio of the difference between spin-up and spin-down currents to the total current at the corresponding peak voltage:

$$P_\pm = \frac{|j_\pm - j_\mp|}{j_\pm + j_\mp}. \quad (16)$$

For the total $I(V)$ (dotted line) in Fig. 5, the first peak yields $\approx$70% spin-down polarization while the second peak delivers $\approx$80% spin-up polarization. The inset shows the calculated spin polarization for each current peak as a function of the

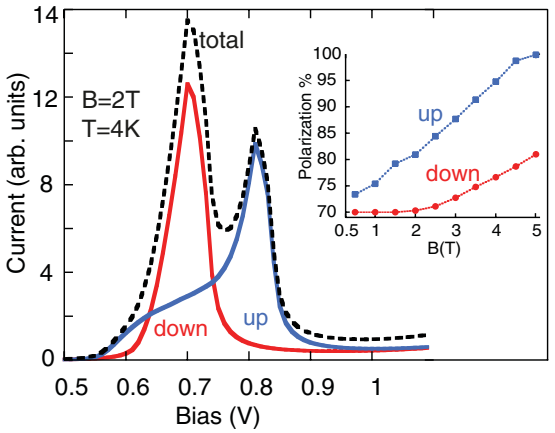

FIG. 5. (Color online) Calculated spin-up, spin-down, and total currents for $B = 2$ T and $T = 4.2$ K. The dotted line corresponds to the total current. The inset shows the current polarization as a function of the magnetic field.

magnetic field. As the figure shows, the spin-up peak always delivers a higher polarization degree. This happens because the spin-down level is already very close to or even below the conduction band edge in the emitter for the voltages demanded by tunneling via the spin-up level. It becomes more evident for large fields when the splitting energy is already comparable to the injection level energy. For such fields, the polarization degree of the second peak can reach virtually 100% while the first peak can yield 80% spin-down polarized currents. Even for small fields ($B = 0.5$ T), the calculations show that the Rashba effect in the tunneling current can provide polarization levels on the order of 70%.

C. Temperature dependence

The temperature influence on the Rashba splitting is displayed in Fig. 6 for $B = 2$ T and $T = 4, 30, 110$, and 180 K. The decreasing peak amplitude with increasing temperatures is a consequence of the temperature-dependent occupation statistics in the emitter electrode. Nevertheless, the most important feature of these calculated $I(V)$ curves is the reduced

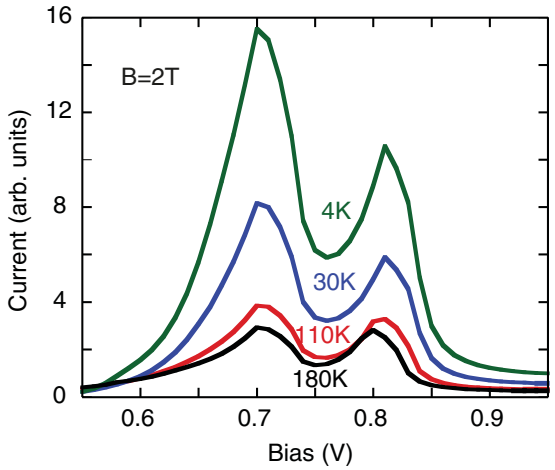

FIG. 6. (Color online) Simulated $I(V)$ curves for temperatures of $T = 4, 30, 110$, and 180 K.

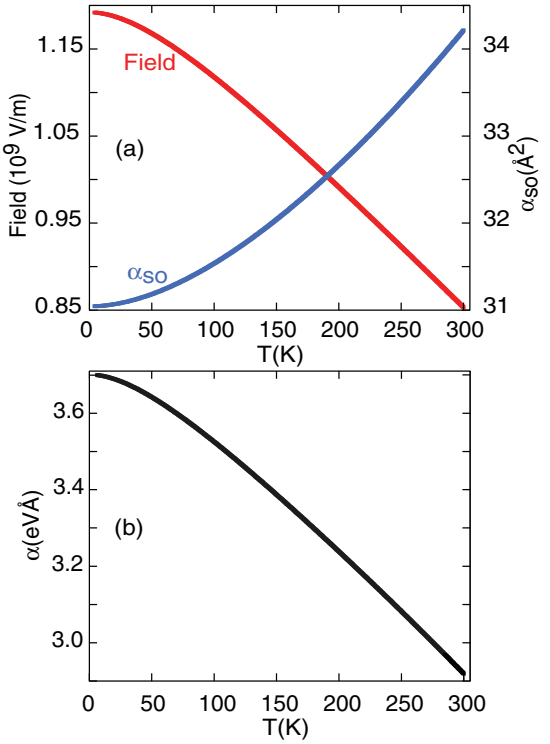

FIG. 7. (Color online) (a) Interface electric field (red) and α_{SO} (blue) and (b) Rashba parameter α as functions of the temperature.

distance between the split peaks as the temperature becomes larger. This is in qualitative agreement with the experimental results (see Fig. 2 in Ref. 8).

The reduced peak distance is a direct result of the influence of the higher temperatures on the Rashba parameter [Eq. (10)]. As a consequence of the temperature increase, the band gap for both materials becomes smaller [Eq. (15)], resulting in a smaller band offset. In our type-II heterostructure, the band offsets in the valence and conduction bands are almost identical. In addition, the energy gaps of InGaAs and GaAsSb are approximately the same. We thus assumed, for simplicity, that the temperature influences the valence and conduction band offsets equally.

The temperature increase influences the Rashba parameter in two ways: (1) by decreasing the band offset and (2) by increasing the α_{SO} term. The smaller band offset yields lower electric fields at the heterostructure interfaces. On the other hand, the α_{SO} term [Eq. (11)] is enlarged by the decrease in band-gap size. In spite of this, the larger α_{SO} is secondary and does not dominate the behavior of the Rashba parameter, and the splitting becomes smaller.

Figure 7(a) shows the interface field and α_{SO} as functions of the temperature. While the interface electric field decreases by around 29% between $T = 4$ and 300 K, α_{SO} increases by only 1%. This is direct evidence that the main influence of the temperature on the interface Rashba parameter comes from the lower interface fields produced by the smaller band offsets. Figure 7(b) displays the product of the interface electric field with α_{SO} (the Rashba parameter) for the bias at resonance ($V = 0.70$ V). The Rashba parameter follows the interface

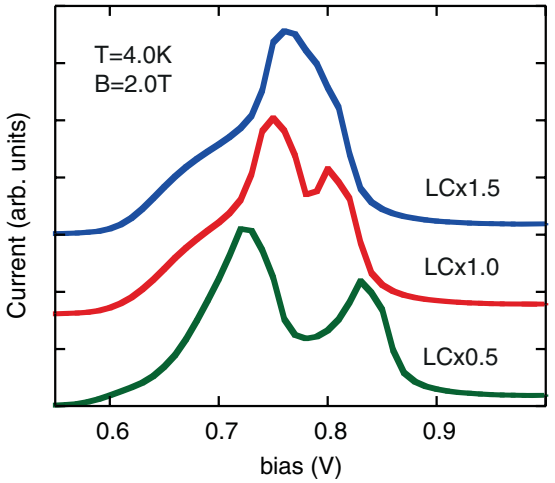

FIG. 8. (Color online) Simulated peak splitting with increasing interface with. LC stands for lattice constant. The external electric fields (dV_{ext}/dz) are taken into consideration in all cases.

electric field tendency and drops from 3.6 eV Åat $T = 4$ K to 2.9 eV Åat $T = 300$ K.

D. Interface-width dependence

As we have shown in Sec. VI C, the main influence on the splitting of the resonance peak comes from the strong electric fields at the interfaces due to the band discontinuities. The interface field is the band offset in the valence band divided by the effective interface width. The interface width is on the order of the distance between the crystal planes, which we consider to be one-half of the lattice constant in GaAsSb (0.586 nm). Further, the electric fields generated by the heterointerfaces in the quantum well are enormous but restricted only to the interface region.

In order to test how sensitive the Rashba splitting is to the interface fields, we calculated the peak splitting assuming larger interface widths. The external fields produced by the applied voltages are also taken into consideration in all calculations. Figure 8 shows what happens to the peak splitting for $B = 2$ T and $T = 4$ K if the interface width is increased. The lowest split resonance is calculated with an interface width of one-half the lattice constant (LC). Note that the resonance splitting becomes considerably smaller when the interface width is considered to be equal to the lattice constant. In the extreme case where the interface width is 1.5 times the LC, the resonance splitting vanishes completely.

E. Effective Rashba parameter

As we have shown above, the electric fields at the interface are the main reason for the peak splitting observed in the resonances. The combination of such electric fields and the α_{SO} coefficients results in especially large Rashba parameters right at the interfaces. Note that the Rashba parameter at the interfaces (Fig. 7) is at least one order of magnitude larger than the usual values reported in the literature for similar materials.[27,28] In addition, the external electric fields generated by the applied bias are on the order of 50 kV/cm. This value times α_{SO} delivers $\alpha \approx 0.02$ eV Å, which is one order of magnitude lower than the values found experimentally for these RTDs [see Ref. 8]. Further, as shown in Fig. 8 the Rashba parameter introduced by the external field alone is not able to produce the observed peak splittings in the simulations for the typical $k_\parallel$ values used in our calculations ($k_\parallel \approx 2 \times 10^8$ m^{-1}).

To remove this apparent discrepancy between the Rashba coefficients obtained from our model and the experimental data, one can define an effective Rashba parameter α_{eff} for this structure as

$$E^{\uparrow} = \alpha_{eff} k_\parallel^{\uparrow}, \qquad E^{\downarrow} = \alpha_{eff} k_\parallel^{\downarrow},$$
$$\alpha_{eff} = \frac{E^{\uparrow} - E^{\downarrow}}{k_\parallel^{\uparrow} - k_\parallel^{\downarrow}}, \quad \alpha_{eff} = \frac{\Delta E}{\Delta k_\parallel}, \tag{17}$$

where ΔE is the resonance peak splitting energy and $k_\parallel^{\uparrow(\downarrow)}$ is the in-plane momentum with largest transmission at the current peak voltage for the respective spin peak.

After using the proper voltage-to-energy conversion (100 mV $\approx$ 10 meV) and taking the values of $k_\parallel$ at which the transmission is maximum around the peak current voltages ($\Delta k_\parallel \approx 2 \times 10^8$ m^{-1} for $B = 2$ T), we get $\alpha = 0.5$ eV Å, which is in excellent agreement with the experimental values calculated in a similar way in Ref. 8.

F. Material comparison: InGaAs/GaAsSb vs GaAs/AlGaAs

In order to investigate why the Rashba splitting is so well resolved in the type-II structure of our calculations, we also ran our simulation for a different material system for a direct comparison. Figure 9 shows the Rashba splitting in GaAsSb/InGaAs compared with the splitting in GaAs/AlGaAs RTDs for the same conditions. In order to make the comparison easier and to show the differences more clearly, we have added an offset to the GaAs/AlGaAs resonance voltage. The valence band offset in this type-I heterostructure was calculated using the widely accepted 60:40 rule. The distance between the split peaks is 129 mV for the GaAsSb/InGaAs RTDs and only 16 mV for GaAs/AlGaAs RTDs, which corresponds to energy splittings of 12.9 and 1.6 meV, respectively.

Even though the electric field magnitudes at the interfaces between the well and the barriers are approximately the same for both systems, the Rashba splitting is almost absent in the GaAs/AlGaAs RTDs. The reason for this is the combination of the large band gap in GaAs/AlGaAs ($E_{gap} \approx 1.4$ eV) with the low spin-orbit gap ($\Delta \approx 0.40$ eV), which leads to an α_{SO} value ten times smaller than what is found in the GaAsSb/InGaAs RTDs. This is in good agreement with the difference in the splitting energy calculated above for the two material systems which is also a factor of 10. In fact, generally, type-II heterojunctions can have the same (or even larger) interface fields as type-I heterojunctions (see Ref. 29 and references therein) with the additional advantage of presenting much smaller band gaps. This gives type-II heterostructures an enormous advantage over type-I heterostructures in producing large and detectable spin-orbit coupling effects in the perpendicular transport case.

Finally, another contribution to the enhancement of the Rashba effect in GaAsSb/InGaAs RTDs is the smaller effective mass of the electrons in aluminum-free materials.[30] The lighter

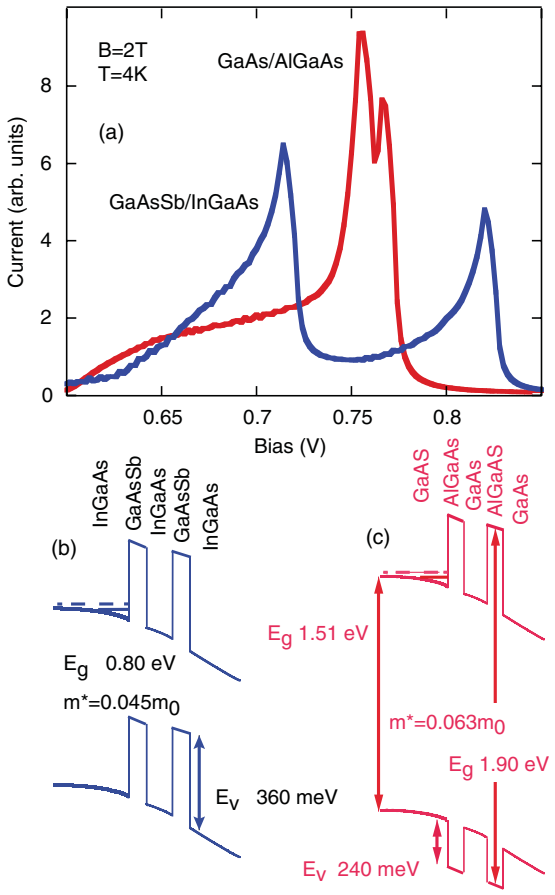

FIG. 9. (Color online) (a) Calculated $I(V)$ curves with Rashba splitting ($B = 2$ T) for GaAsSb/InGaAs and GaAs/AlGaAs RTDs. Red curve, GaAsSb/InGaAs; blue curve (with a bias offset), GaAs/AlGaAs. (b) Type-II band profile of the GaAsSb/InGaAs heterostructure. (c) Type-I band profile of the GaAs/AlGaAs heterostructure. The aluminum concentration is 40%. The figure displays the main parameters used in the calculations.

electrons shift the resonances to higher voltages and hence to higher k_z momentum. This leads to larger values for the in-plane momentum since the Lorentz forces are directly proportional to the energies in the z direction.

VII. SUMMARY

In summary, we investigated via the TMM spin-orbit coupling effects in perpendicular transport under the influence of transverse magnetic fields and the Rashba effect. Our calculations showed that the Rashba effect in a GaAsSb/InGaAs RTD can be enhanced by an in-plane magnetic field and their results are in excellent agreement with those of previously reported experiments.[8] The predicted levels of spin-polarized currents are extremely large even for fields below $B = 1$ T although no resonance splitting can be seen for such low magnetic fields. The temperature dependence of the Rashba parameter introduced in the model via the band gap reproduced very well the decrease of peak splitting observed in the experiment. Clearly, the calculations show that the Rashba parameter can still be large even at room temperature and that the Rashba effect can be observed for temperatures above 180 K. These results depend on the resistance of the RTD's peak-to-valley ratio to a temperature increase.

The main finding of our calculations is the extreme dependence of the Rashba effect on the electric fields generated at the interfaces by the band discontinuity. The combination of large Rashba parameters and the in-plane acceleration produced by the magnetic fields results in a strongly spin-controlled scattering mechanism at the quantum well interfaces. This influences the transmission coefficient for the whole structure and produces one current resonance peak for each spin state. In this case, the net Rashba parameter is an average of all scattering processes that contribute to the current. We defined an effective Rashba parameter based on the energy separation between the resonance peaks and the in-plane momentum $k_{\|}$ of electrons with maximum transmission at the current peak. The value we found ($\alpha = 0.5$ eV Å) is in excellent agreement with our experiments.

From this model, one can predict how interfaces for optimized spin splitting should look. First, the molecular-beam epitaxial (MBE) growth should be well controlled and produce sharp interfaces. Second, by a change in the InGaAs or GaAsSb composition, the valence band offsets can be tuned. A larger band offset should increase the Rashba effect. However, one should do it by decreasing the energy gap of InGaAs to keep the α_{SO} parameter large. Testing if this is realistic will be a challenge in the field of MBE growth. We must emphasize that α_{SO} is on the order of 40 Å^2 in InGaAs/GaAsSb RTDs, which is an order of magnitude larger than α_{SO} in GaAs. This is certainly one of the reasons that the Rashba effect is so pronounced in this material system even at high temperatures, since large band offsets are not hard to produce. Some other materials such as InAs and InSb can present an α_{SO} coefficient up to ten times larger than that in InGaAs.[12] The combination of even larger α_{SO} materials with large band offsets for an RTD could obviously increase the Rashba effect and make it observable probably even at room temperature.

ACKNOWLEDGMENTS

This work was sponsored by FWF-Austria, Projects No. SFB-25-03 and SFB-25-08 (IR-ON). Further, the authors are especially thankful to Erich Gornik for valuable discussions and his support over so many years.

*jonathan.sousa@tuwien.ac.at

[1] S. A. Wolf, D. D. Awschalom, R. A. Buhrman, J. M. Daughton, S. von Molnar, M. L. Roukes, A. Y. Chtchelkanova, and D. M. Treger, Science **294**, 1488 (2001).

[2] S. A. Wolf, A. Chtchelkanova, and D. Treger, IBM J. Res. Dev. **50**, 101 (2006).

[3] D. D. Awschalom and M. Flatté, Nat. Phys. 3, 153 (2007).

[4] T. Koga, J. Nitta, H. Takayanagi, and S. Datta, Phys. Rev. Lett. **88**, 126601 (2002).

[5] S. Datta and B. Das, Appl. Phys. Lett. **56**, 665 (1990).

[6] E. I. Rashba and F. T. Tela, Sov. Phys. Solid State **2**, 1109 (1960).

[7]Y. A. Bychkov and E. Rashba, Pis'ma Zh. Eksp. Teor. Fiz. **39**, 66 (1984).
[8]J. S. de Sousa, H. Detz, P. Klang, E. Gornik, G. Strasser, and J. Smoliner, Appl. Phys. Lett. **99**, 152107 (2011).
[9]R. Tsu and L. Esaki, Appl. Phys. Lett. **22**, 562 (1973).
[10]J. S. de Sousa, H. Detz, P. Klang, M. Nobile, A. M. Andrews, W. Schrenk, E. Gornik, G. Strasser, and J. Smoliner, J. Appl. Phys. **108**, 073707 (2010).
[11]D. F. Nelson, R. C. Miller, and D. A. Kleinman, Phys. Rev. B **35**, 7770 (1987).
[12]E. A. de Andrada e Silva, G. C. La Rocca, and F. Bassani, Phys. Rev. B **55**, 16293 (1997).
[13]G. Snider, [http://www.nd.edu/gsnider/].
[14]G. Feve, W. D. Oliver, M. Aranzana, and Y. Yamamoto, Phys. Rev. B **66**, 155328 (2002).
[15]W. Knap, C. Skierbiszewski, A. Zduniak, E. Litwin-Staszewska, D. Bertho, F. Kobbi, J. L. Robert, G. E. Pikus, F. G. Pikus, S. V. Iordanskii, V. Mosser, K. Zekentes, and Y. B. Lyanda-Geller, Phys. Rev. B **53**, 3912 (1996).
[16]J. Smoliner, D. Rakoczy, and M. Kast, Rep. Prog. Phys. **67**, 1863 (2004).
[17]D. Rakoczy, J. Smoliner, R. Heer, and G. Strasser, J. Appl. Phys. **88**, 3495 (2000).
[18]E. A. de Andrada e Silva, G. C. La Rocca, and F. Bassani, Phys. Rev. B **50**, 8523 (1994).
[19]R. Lassnig, Phys. Rev. B **31**, 8076 (1985).
[20]Y. Varshni, Physica **34**, 149 (1967).
[21][http://www.ioffe.rssi.ru/SVA/NSM/Semicond/index.html].
[22]M. Karatchevtseva, A. Ignatiev, V. G. Mokerov, G. S. Nemtsov, V. A. Strakhov, and N. G. Yaremenko, Semiconductors **28**, 691 (1994).
[23]K. G. Merkel, V. M. Bright, M. A. Marciniak, C. L. A. Cerny, and M. O. Manasreh, Appl. Phys. Lett. **65**, 2442 (1994).
[24]D. Z.-Y. Ting and X. Cartoixà, Phys. Rev. B **68**, 235320 (2003).
[25]A. Voskoboynikov, S. S. Lin, C. P. Lee, and O. Tretyak, J. Appl. Phys. **87**, 387 (2000).
[26]E. A. de Andrada e Silva and G. C. La Rocca, Phys. Rev. B **59**, R15583 (1999).
[27]D. Grundler, Phys. Rev. Lett. **84**, 6074 (2000).
[28]T. Schäpers, G. Engels, J. Lange, T. Klocke, M. Hollfelder, and H. Lüth, J. Appl. Phys. **83**, 4324 (1998)
[29]M. P. Mikhailova, K. D. Moiseev, and Y. P. Yakovlev, Semicond. Sci. Technol. **19**, R109 (2004).
[30]M. Nobile, P. Klang, E. Mujagic, H. Detz, A. Andrews, W. Schrenk, and G. Strasser, Electron. Lett. **45**, 1031 (2009).